Physics and Chemistry of Minerals (2022) 49:11
https://doi.org/10.1007/s00269-022-01188-4

ORIGINAL PAPER

The electrical conductivity of Fe_4O_5, Fe_5O_6, and Fe_7O_9 up to 60 GPa

Shuhou Maitani[1] · Ryosuke Sinmyo[1] · Takayuki Ishii[2,3] · Saori I. Kawaguchi[4] · Naohisa Hirao[4]

Received: 29 September 2021 / Accepted: 22 December 2021

Abstract
The electrical conductivities of iron-bearing minerals are important for understanding the chemical and thermal heterogeneity of the Earth's mantle. Recent high-pressure experiments have shown that the new iron oxide group $(FeO)_m(Fe_2O_3)_n$ is stable under mantle conditions. Although the new iron oxides possibly play an important role in the subduction zone, the physical properties of these iron oxides are still unclear. Here, we determined the electrical conductivities of Fe_4O_5, Fe_5O_6, and Fe_7O_9 at pressures up to 60 GPa using diamond anvil cells. The electrical conductivities of the iron oxides generally increased with increasing pressure, and the values were comparable with previous data for Fe_3O_4 and FeO at high pressures. Although iron oxides with a mixed-valence state are generally highly conductive, Fe_7O_9 was less conductive than Fe_4O_5 and Fe_5O_6. This difference is likely due to the ordered sites and valences in the structures of Fe_4O_5 and Fe_5O_6. The results show that the new iron oxides were not metallic under the experimental conditions. The iron oxides in the subducted materials may cause anomalies in the electrical conductivity of the deep mantle along with the melt and water.

Keywords Iron oxide · Electrical conductivity · Mantle

Introduction

Iron is the third most abundant cation in the Earth's mantle. Because iron has a strong effect on electromagnetic properties, researchers have long studied the electrical conductivities of iron-bearing minerals to understand the chemical and thermal heterogeneity of the crust and mantle. Electrical conductivities are generally higher in rocks with higher concentrations of water, melt, and iron in the minerals (Yoshino 2010; Katsura et al. 2017). For instance, the observed conductivity of the transition zone (410–660 km depth) is consistent with those of $(Mg, Fe)_2SiO_4$ ringwoodite and wadsleyite with Mg# ~ 90 (Yoshino and Katsura 2009; Yoshino 2010). The valence state of iron also strongly affects the conductivity of minerals (Tannhauser 1962; Xu et al. 1998; Potapkin et al. 2013). The electrical conductivity of Fe_3O_4 magnetite (Fe^{3+}/total Fe = 2/3) is several tens of times higher than that of Fe_2O_3 hematite (Fe^{3+}/total Fe = 1) (Tannhauser 1962). Although olivine, wadsleyite, and ringwoodite can hardly accommodate Fe^{3+}, Al-bearing bridgmanite and majorite-garnet contain a considerable amount of Fe^{3+} even under reducing conditions via the disproportionation reactions $3Fe^{2+} = 2Fe^{3+} + Fe^0$ (Frost et al. 2004; Rohrbach et al. 2007). The electrical conductivities of olivine, wadsleyite, and ringwoodite are much lower than those of iron oxides (Yoshino and Katsura 2009). In contrast, the electrical conductivities of Al-bearing bridgmanite and majorite-garnet are relatively high (Yoshino et al. 2008).

Although iron oxides are not the main constituent minerals of the average mantle (McCammon 2005; Irifune et al. 2010), iron oxides may play an important role in the subduction process, which delivers relatively hydrated and oxidized materials into the deep mantle. It has been suggested that Fe_3O_4 magnetite is formed via the serpentinization process at

This article is part of a Topical Collection "Experimental & Analytical Techniques at Extreme & Ambient Conditions", guest edited by Stella Chariton, Vitali B. Prakapenka and Haozhe (Arthur) Liu.

✉ Shuhou Maitani
ce217019@meiji.ac.jp

[1] Department of Physics, School of Science and Technology, Meiji University, 1-1-1 Higashi Mita, Tama-ku, Kawasaki, Kanagawa 214-8571, Japan

[2] Center for High Pressure Science and Technology Advanced Research, Beijing 100094, China

[3] Bayerisches Geoinstitut, Universitaet Bayreuth, 95440 Bayreuth, Germany

[4] Japan Synchrotron Radiation Research Institute, 1-1-1 Koto, Sayo, Hyogo 679-5198, Japan

Published online: 03 May 2022

the mantle wedge and corresponds to the observed anomaly in magnetism (Blakely et al. 2005). In addition, subducted Fe^{3+}-rich banded iron formation (BIF) may cause a wide variation in the oxygen fugacity of the deep mantle (Dobson and Brodholt 2005; Kang and Schmidt 2017). Indeed, recent studies have suggested that the deep mantle has much wider variations in oxygen fugacity based on observations from diamond inclusions and peridotites (Stagno et al. 2013; Wirth et al. 2014; Kaminsky et al. 2015; Kagi et al. 2016; Smith et al. 2016; Kiseeva et al. 2018). The oxygen fugacity of peridotite decreases with increasing depth to ~ 200 km from the quartz–fayalite–magnetite (QFM) buffer to three log units below QFM (Stagno et al. 2013). While determining the oxygen fugacity of the mantle deeper than 200 km is not straightforward, the electrical conductivity can provide important information for understanding the oxygen fugacity of the deep mantle. The observed lateral variation in the electrical conductivity (Püthe and Kuvshinov 2013; Katsura and Yoshino 2015) may be attributed to the anomaly in the oxygen fugacity in addition to water, high temperature, and melting. However, the electrical conductivities of iron oxides are not yet well understood at high pressures.

While minerals with the stoichiometry of FeO, Fe_2O_3, and Fe_3O_4 are stable at ambient pressures, recent studies have shown the occurrence of a new iron oxide group $(FeO)_m(Fe_2O_3)_n$ that is stable above ~ 10 GPa, corresponding to the upper mantle conditions. The group includes Fe_4O_5, Fe_5O_6, Fe_7O_9, Fe_9O_{11}, Fe_5O_7, $Fe_{13}O_{19}$, and $Fe_{25}O_{32}$ (Lavina et al. 2011, 2015; Merlini et al. 2015; Bykova et al. 2016; Sinmyo et al. 2016; Ishii et al. 2018). All iron oxides above are likely metastable at ambient pressures, including the Fe_4O_5, Fe_5O_6, and Fe_7O_9 used in this study. Previous studies have shown that Fe_4O_5 and Fe_5O_6 are stable at pressures above approximately 10 GPa and at relatively high-oxygen fugacity conditions (Woodland et al. 2013; Myhill et al. 2016; Uenver-Thiele et al. 2018), and Fe_7O_9 is suggested to be stable at even higher pressures, likely above 25 GPa (Sinmyo et al. 2016). The $(FeO)_m(Fe_2O_3)_n$ iron oxides are composed of a combination of FeO_6-octahedral and FeO_6-trigonal prisms (Bykova et al. 2016). According to thermodynamic modeling, Fe_5O_6 can coexist with diamond above ~ 10 GPa at 1473 K (Myhill et al. 2016). This suggests that the high-pressure iron oxide phases can be trapped inside diamond inclusions (Wirth et al. 2014; Kaminsky et al. 2015). Indeed, a recent study showed the possible relics of Fe_4O_5 in diamond inclusions delivered from the deep mantle (Anzolini et al. 2020). To understand the stability of Fe_4O_5 and Fe_5O_6, high-pressure experiments were conducted using a multi-anvil press and a diamond anvil cell with X-ray diffraction (XRD) measurements (Woodland et al. 2013; Myhill et al. 2016; Uenver-Thiele et al. 2018; Hikosaka et al. 2019). In contrast to the phase stability, the physical properties of the iron oxides, such as their electrical conductivities, are currently poorly understood (2016, 2020).

The electrical conductivities of the iron oxides are remarkably different based on the crystal structure and valence state of the iron. The electrical conductivities of $Fe_{1-x}O$ wüstite and Fe_3O_4 magnetite are several tens of times higher than that of Fe_2O_3 hematite at ambient pressure (Tannhauser 1962). Pasternak et al. (1999) showed that the conductivity of Fe_2O_3 significantly increases above ~ 50 GPa, likely because of the transition of its phase to its high-pressure polymorph with a Rh_2O_3-type structure. More recently, Bykova et al. (2016) showed that Fe_2O_3 exhibits various polymorphs, such as a distorted perovskite structure (ζ-Fe_2O_3) and post-perovskite structure (η-Fe_2O_3), at pressures above ~ 50 GPa in addition to Rh_2O_3-type structures. In contrast, the electrical conductivity of Fe_3O_4 decreases above ~ 20 GPa because of the phase transition to the high-pressure polymorph (Morris and Williams 1997). FeO, with a rock salt-type structure, undergoes an insulator-to-metallic transition at 70 GPa and 1900 K (Ohta et al. 2012). FeO, with a B8-type structure, is stable above ~ 80 GPa and is a metallic phase (Ohta et al. 2010). It was shown that the magnetism of FeO collapsed at approximately 50 GPa by means of Mössbauer spectroscopy (Pasternak et al. 1997). A recent study by Hamada et al. (2016) showed that the magnetic high-spin component of $Fe_{0.96}O$ decreased gradually with increasing pressure from 91 to 203 GPa. Recent studies have suggested that the observed anomalies in magnetism around the subduction zone (Blakely et al. 2005) may correspond to Fe_2O_3 hematite under high-pressure and relatively low-temperature conditions (Kupenko et al. 2019). Previous studies have suggested that the ordering of the valence state in the chain of the FeO_6 octahedra enhances the electrical conductivity of Fe_4O_5 and Fe_5O_6 (Ovsyannikov et al. 2016, 2020). It has also been reported that the electrical conductivities of Fe_4O_5 and Fe_5O_6 have kinks at 150 and 275 K, respectively (Ovsyannikov et al. 2016, 2020). Theoretical calculations suggest that Fe_4O_5 is metallic from ambient to high-pressure conditions (Yang et al. 2021). However, the prediction contradicts experimental work showing a higher conductivity of Fe_4O_5 at a higher temperature (Ovsyannikov et al. 2016), which is not plausible for the electronic conduction mechanism in the metallic phase. The electrical conductivity of (Mg, Fe)O ferropericlase decreases above 30–60 GPa due to high-spin to low-spin crossover (Ohta et al. 2007; Yoshino 2010). Based on the unit cell volume decrease, the iron may undergo a high-spin to low-spin crossover at approximately 40 GPa in Fe_4O_5 (Hikosaka et al. 2019).

In this study, we determined the electrical conductivities of Fe_4O_5, Fe_5O_6, and Fe_7O_9 up to 60 GPa for the first time. The electrical conductivities of these iron oxides generally increase with increasing pressure. The results showed that the iron oxides were not in metallic phases under the experimental conditions. Because the iron oxides are highly conductive, the anomaly in the electrical conductivity observed under the deep mantle can be explained by the presence of a small amount of iron oxide.

Experiments

We used Fe_4O_5, Fe_5O_6, and Fe_7O_9 as starting materials; they were synthesized from a mixture of reagent grade Fe metal and Fe_3O_4 or Fe_2O_3 powders using a 15-MN Kawai-type multi-anvil press with the Osugi-type module (IRIS-15) at the Bayerisches Geoinstitut (Ishii et al. 2016, 2019). We synthesized Fe_4O_5, Fe_5O_6, and Fe_7O_9 at 15 GPa/1700 K, 10 GPa/1700 K, and 25 GPa/1973 K, respectively. The phases were characterized using XRD (Fig. 1). The Fe_4O_5 and Fe_5O_6 samples were analyzed using micro-focused X-ray diffractometers with a target of Co (Bruker, D8 Discover) and Mo (Bruker, D8 Venture), respectively. The Fe_7O_9 sample was measured using a Bruker X-ray diffractometer equipped with a SMART APEX CCD detector with a high-brilliance Rigaku rotating anode (Rotor Flex FR-D, Mo-Kα radiation).

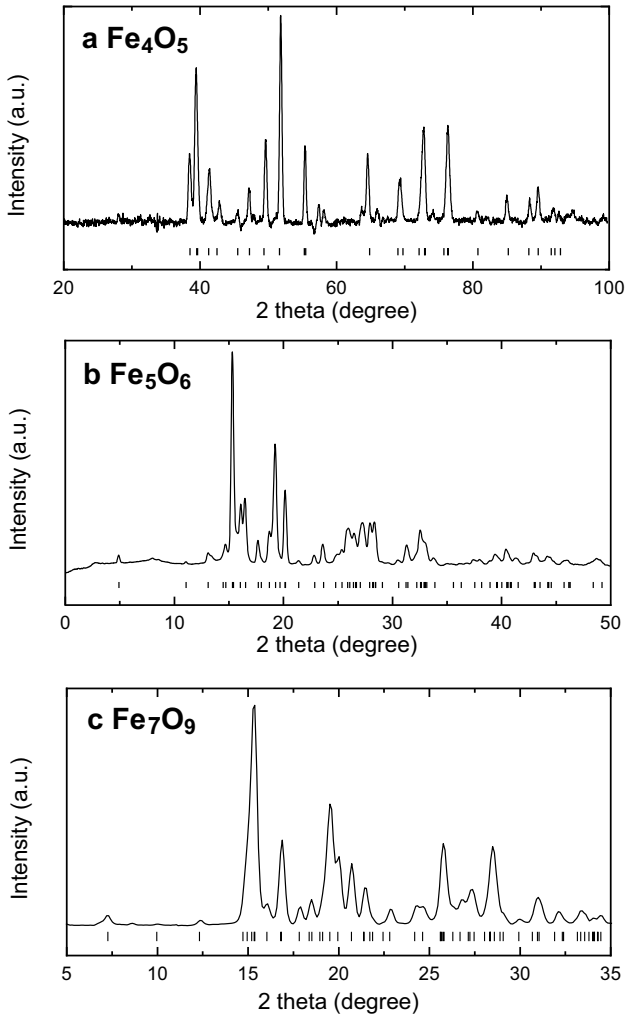

Fig. 1 X-ray diffraction patterns of **a** Fe_4O_5, **b** Fe_5O_6, and **c** Fe_7O_9 obtained in ambient conditions. The bars under the spectra are the predicted value for each phase

The electrical resistances of the samples were measured under high-pressure conditions using diamond anvil cells. Diamonds with 300 or 450 μm culet diameters were used for the anvils. We drilled a 250 or 375 μm diameter hole in the rhenium plate, which was compressed to a thickness of approximately 50 μm. An electrical insulator (c-BN) was filled into the hole in the rhenium plate and then compressed again to a thickness of 50 μm. Holes 80–120 μm in diameter were drilled in the insulation layer. The sample was placed in the hole, and four platinum foils of 7.5 μm thickness were placed on the sample as electrodes (Fig. S1). The electrical resistances were measured by a quasi-four-terminal method using a multimeter.

Determination of the electrical conductivity from the measured resistance values requires the thickness, width, and length of the sample. The width and length were determined by optical observation using a microscope with an uncertainty of ~ 10%. To estimate the thickness of the sample, we used the relationship between pressure and the anvil gap proposed by Sinmyo et al. (2014). In run #3, the thickness of the recovered sample was determined by electron microscopy, and the results were consistent with the estimation. The uncertainty in the thickness was assumed to be 50%, and the propagated uncertainty of the conductivity was estimated to be 52%. Because the thickness was estimated from the literature data, the error represents the possible shift of the conductivity for each run relative to other runs. The conductivities of the samples were measured at high pressures of up to 60 GPa (Fig. 2). In addition

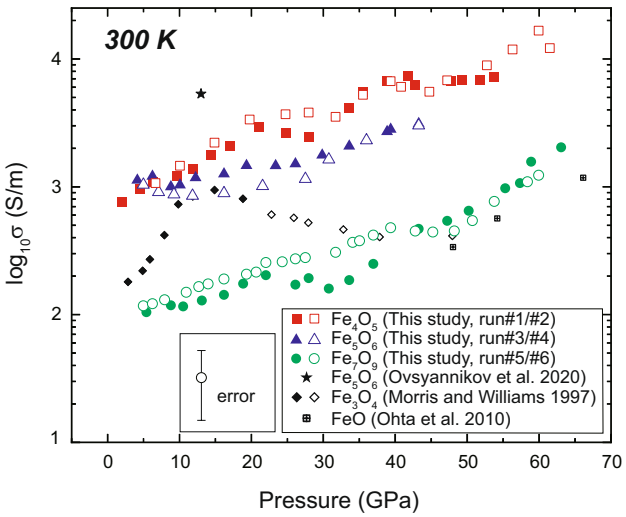

Fig. 2 The relationships between pressure and the electrical conductivities of iron oxides at ambient temperature. The data for Fe_4O_5 (red squares), Fe_5O_6 (blue triangles), and Fe_7O_9 (green circles) were obtained in this study. Diamonds are low-pressure (filled diamonds) and high-pressure polymorph (open diamonds) of Fe_3O_4 (Morris and Williams 1997). Results from previous studies on Fe_5O_6 (Ovsyannikov et al. 2020) and FeO (Ohta et al. 2010) are also shown

to the experiments at room temperature, the samples were cooled to ~ 80 K under selected pressure conditions to estimate the activation enthalpies of Fe_4O_5 (run #1), Fe_5O_6 (run #4), and Fe_7O_9 (run #6). The electrical conductivity was measured every +/− 1 K during the heating/cooling process (Fig. 3). In run #6, the temperature ranges were limited to 260–300 K, because the thermocouples failed during the experiments. The resistances were monitored during both cooling and heating processes. We also measured the conductivities at high temperatures for run #3 by placing the whole cell in the furnace. The temperatures were monitored using thermocouples attached to the diamond anvil. The pressure was determined at 300 K using the Raman spectra of the diamond anvil (Akahama and Kawamura 2004).

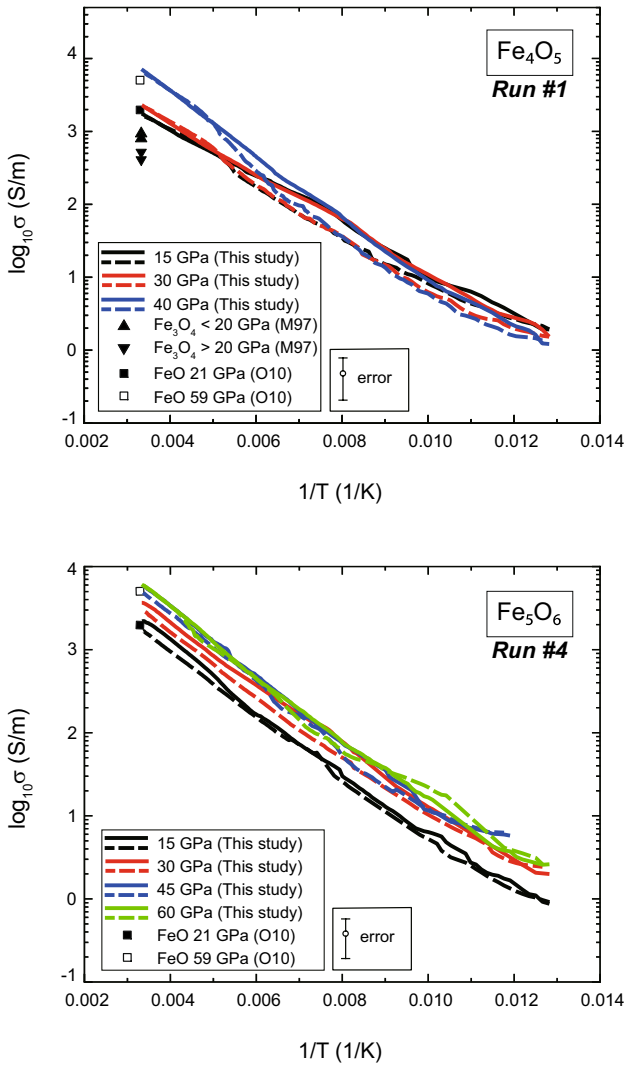

Fig. 3 The conductivity of Fe_4O_5 (upper) and Fe_5O_6 (lower) against reciprocal temperature at high pressure. Data were obtained during cooling (solid lines) and heating (broken lines). Results from previous studies are also shown for comparison. M97 and O10 denote data by Morris and Williams (1997) and Ohta et al. (2010), respectively. Errors were estimated by the same manner with Fig. 2

Results

The XRD measurements showed that the samples were single phases of Fe_4O_5, Fe_5O_6, and Fe_7O_9 (Fig. 1). The obtained unit cell parameters were consistent with those of previous studies (Lavina et al. 2011, 2015; Sinmyo et al. 2016). We carried out six sets of runs to determine the electrical conductivities of Fe_4O_5, Fe_5O_6, and Fe_7O_9 at high pressures up to 60 GPa (Fig. 2). Two runs were conducted in each phase, and the obtained data showed high reproducibility (Fig. 2). The conductivities of Fe_4O_5, Fe_5O_6, and Fe_7O_9 were generally close to those of FeO, Fe_3O_4, and Fe_4O_5 reported in previous studies (Morris and Williams 1997; Ohta et al. 2010; Ovsyannikov et al. 2020). The electrical conductivities increased with increasing pressure (Fig. 2). The relationships between the conductivity ($\log_{10}\sigma$) and reciprocal of temperature ($1/T$) are shown in Fig. 3. While we also plotted $\log_{10}(\sigma^*T)$ against $1/T$ for comparison, the obtained curves were quite similar to those obtained using $\log_{10}\sigma$ (Fig. S2). The electrical conductivities were fitted using the following equation:

$$\sigma = \sigma_0 \exp\left(-\frac{\Delta H}{kT}\right), \quad (1)$$

where σ is the electrical conductivity, σ_0 is the conductivity at an infinite temperature, ΔH is the activation enthalpy, k is the Boltzmann constant, and T is the temperature. The activation enthalpies were ~ 0.1 eV in Fe_4O_5, Fe_5O_6, and Fe_7O_9 (Fig. 4). The Fe_5O_6 sample was heated to 370 K at 15 GPa in run #3. The conductivity value increased by 50% at 360 K upon heating. Since the change was irreversible, Fe_5O_6 was likely transformed to other iron oxides, such as $FeO + Fe_4O_5$ at 360 K, as suggested by a previous study (Hikosaka et al. 2019). Indeed, the conductivity of Fe_4O_5 was ~ 2 times higher than that of Fe_5O_6 at 15 GPa and 300 K (Fig. 2). Although we conducted the measurement without using a pressure medium, the sample and electrode were not largely deformed from the initial geometry.

Discussion

We summarized the relationship between the pressure and electrical conductivity for Fe_4O_5, Fe_5O_6, and Fe_7O_9 at 300 K (Fig. 2). The electrical conductivity of Fe_5O_6 was comparable to that reported in a previous study (Ovsyannikov et al. 2020). While it is known that the conductivities of FeO wüstite and Fe_3O_4 magnetite are several tens of times higher than that of Fe_2O_3 hematite at ambient pressure

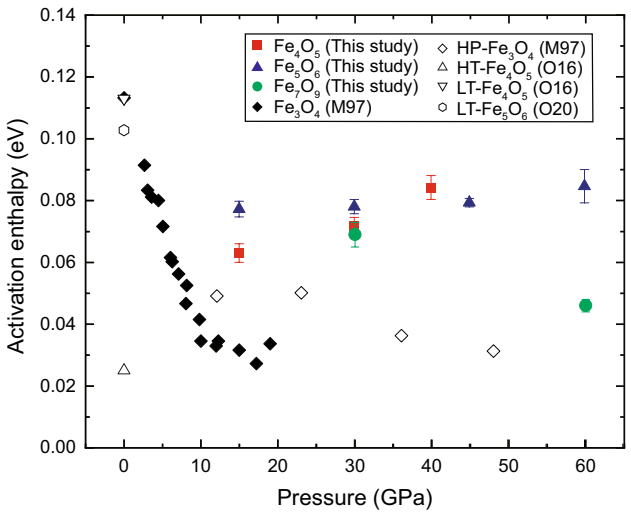

Fig. 4 Activation enthalpy of iron oxides at high pressure. M97, O16, and O20 are data taken from Morris and Williams (1997) and Ovsyannikov et al. (2016, 2020), respectively

(Tannhauser 1962), the conductivities of Fe_4O_5 and Fe_5O_6 are as high as those of FeO and Fe_3O_4. This may correspond to the mixed-valence state of iron in Fe_4O_5 and Fe_5O_6. In contrast, the conductivity of Fe_7O_9 is approximately one order of magnitude lower than those of Fe_4O_5 and Fe_5O_6, although Fe_7O_9 contains both Fe^{3+} and Fe^{2+}. This is likely due to the difference in the crystallographic site and valence state of iron. It has been reported that the ordering in the charge and electron orbitals of iron dominantly controls the electrical conductivity of Fe_3O_4 and Fe_4O_5 (Senn et al. 2012; Ovsyannikov et al. 2016, 2020). Ovsyannikov et al. (2016) suggested that dimeric and trimeric ordering in the chain of the FeO_6 octahedra enhance the electrical conductivity. Such chains are not abundant in the structure of Fe_7O_9 compared to those in the structures of Fe_4O_5 and Fe_5O_6. FeO_6 octahedra share edges, forming a chain along the *a*-axis of Fe_4O_5/Fe_5O_6 and *b*-axis of the Fe_7O_9. In Fe_4O_5 and Fe_5O_6, all chains further share edges to form zigzag chains along the *b*-axis. Such zig–zag chains are less abundant along the *a*-axis of Fe_7O_9 compared to Fe_4O_5 and Fe_5O_6 (Sinmyo et al. 2016). This difference may be a reason for the low conductivity of Fe_7O_9. If this is the case, other iron oxides that lack the chain of FeO_6 octahedra, such as Fe_5O_7, $Fe_{13}O_{19}$, and $Fe_{25}O_{32}$, may also be less conductive. To test this hypothesis, their conductivities should be measured along different crystal orientations, although it is challenging to synthesize large single crystals. In addition, the lattice preferred orientation may take place by uniaxial compression. Further studies are necessary to be conducted at hydrostatic conditions.

The electrical conductivities of Fe_4O_5, Fe_5O_6, and Fe_7O_9 generally increased with increasing pressure (Fig. 2). A previous study suggested a high-spin to low-spin crossover of iron in Fe_4O_5 at approximately 40 GPa based on the decrease in unit cell volume (Hikosaka et al. 2019). By an analogy of the FeO and (Mg,Fe)O (Ohta et al. 2007; Yoshino 2010), the electrical conductivity of Fe_4O_5 may be changed at 40 GPa owing to the spin crossover. The fitted results showed that the slope of the conductivity was $d(\log\sigma)/dP = 0.02$ S/GPa below 40 GPa, and was 0.03 S/GPa above 40 GPa, respectively. This suggests that the conductivity is weakly influenced by the spin crossover of iron in Fe_4O_5. Because the difference is not significant, the conduction mechanism may not change. The decrease in the unit cell volume may cause a change in the activation volume, which controls the slope of the conductivity (Hikosaka et al. 2019). However, because of the relatively high uncertainty in this study, further discussion of the transition is not straightforward. The spin state of iron should be studied further by X-ray emission spectroscopy and Mössbauer spectroscopy.

We summarized the relationship between the temperature and the electrical conductivity for Fe_4O_5, Fe_5O_6, and Fe_7O_9 at pressures from 15 to 60 GPa (Fig. 3 and S2). The electrical conductivity slightly increased with increasing temperature in Fe_4O_5, Fe_5O_6, and Fe_7O_9 under the experimental conditions. Although a recent study suggested that Fe_4O_5 is metallic from ambient to high-pressure conditions (Yang et al. 2021), the current results indicate that Fe_4O_5 is not a metallic phase, as shown previously (Ovsyannikov et al. 2016). While the reason for this discrepancy between theory and experiments is not clear, it has been suggested that the metallic ground state in ferropericlase may have been incorrectly predicted, which depends on the assumptions used in the theoretical calculations (Tsuchiya et al. 2006).

Yoshino et al. (2016) discussed the electrical conduction mechanism of Fe^{3+}-bearing $MgSiO_3$-rich bridgmanite by comparing $\log_{10}(\sigma^*T)$ and $\log_{10}(\sigma)$ against $1/T$. The results suggest that the small polaron/ionic conduction is the dominant mechanism at low and high temperatures. However, we obtained similar $\log_{10}(\sigma^*T)$ and $\log_{10}(\sigma)$ for Fe_4O_5 and Fe_5O_6 (Fig. S2), likely because of the relatively narrow temperature range. Although it is not easy to determine the conduction mechanisms of the iron oxides, by an analogy of the Fe^{3+}-bearing (Mg,Fe)O, the small polaron conduction may be the dominant mechanism in $(FeO)_m(Fe_2O_3)_n$ at temperatures below ~ 1000 K (Dobson et al. 1997). The conduction mechanisms of iron oxides should be studied further through high-temperature experiments. We noted that the $\log_{10}(\sigma^*T)$ and $\log_{10}(\sigma)$ deviated from the linear trend at temperatures lower than the magnetic phase transition temperature in previous studies (Fig. S2) (Ovsyannikov et al. 2016; 2020). The transition temperature in Fe_4O_5 increased from 90 to 100 K as the pressure changed from 30 to 40 GPa, and in Fe_5O_6, it increased from 90 to 100 K as the pressure changed from 15 to 60 GPa.

The activation enthalpies of Fe_4O_5, Fe_5O_6, and Fe_7O_9 were between 50–90 meV at pressures between 15 and 60 GPa (Fig. 4). These values are comparable with those reported in previous studies on Fe_4O_5 and Fe_5O_6 at 1 atm (Ovsyannikov et al. 2016, 2020). The values correspond to the bandgap of 100–180 meV, assuming that the bandgap is double the activation energy (Ovsyannikov et al. 2016, 2020). These values are comparable to those of magnetite (70 meV) below the temperature of the Verwey transition (Chainani et al. 1995). A previous study suggested that the activation enthalpy of a high-pressure polymorph of Fe_3O_4 increases with increasing pressure up to 50 GPa, in contrast to Fe_3O_4 magnetite below 20 GPa (Morris and Williams 1997). The pressure dependence of the activation enthalpies of Fe_4O_5, Fe_5O_6, and Fe_7O_9 was close to the high-pressure polymorph of Fe_3O_4. While the crystal structure was not determined in the earlier study (Morris and Williams 1997), the crystal structure of the high-pressure Fe_3O_4 phase is similar to that of the $(FeO)_m(Fe_2O_3)_n$ group with two FeO_6-octahedral sites (Fei et al. 1999; Bykova et al. 2016; Sinmyo et al. 2016).

Based on the obtained data, we have extrapolated the conductivity of Fe_4O_5 and Fe_5O_6 to 13–21 GPa and 1800–1990 K, corresponding to the condition at 400–600 km depth (Katsura et al. 2010). We used Eq. (1) with obtained activation enthalpy for extrapolation (Fig. 4), assuming that the conduction mechanism does not change at high temperatures.

The conductivities of Fe_4O_5 and Fe_5O_6 at 400 km depth are 3×10^4 and 2×10^4 S/m, respectively, and the values are almost the same at a depth of 600 km. For comparison, we also estimated the bulk conductivity of pyrolite at a depth of 600 km based on the electrical conductivities and unit cell volume of ringwoodite and garnet reported in previous studies (Meng et al. 1994; Wang et al. 1998; Yoshino et al. 2008). The bulk conductivity of the pyrolite was estimated to be 0.3 S/m at a depth of 600 km using the Voigt–Reuss–Hill average. A previous study suggested that the electrical conductivity at depths between 400 and 600 km has lateral variations from 0.1 to 1 S/m (Püthe and Kuvshinov 2013). Because the iron oxides are highly conductive, pyrolite + ~0.1% of Fe_4O_5 or Fe_5O_6 can explain the high conductivity of 1 S/m at a depth of 600 km. This suggests that the high-pressure polymorph of iron oxides can be a possible source of the high conductivity anomaly. However, the conductivity of rocks strongly depends on the connectivity of the constituent minerals. A minor phase with 0.1% abundance may have an influence on the bulk conductivity, only if the phase has a sufficiently low viscosity to form a connected network. Rheological parameters of the iron oxides, such as their viscosity and wet angle, should be determined to understand the connectivity. Moreover, their electrical conductivity should be studied further at higher temperatures with phase identification using in situ XRD measurements because the stabilities of the iron oxides are still not clear. Previous studies have shown that Fe_4O_5, Fe_5O_6, Fe_7O_9, and Fe_9O_{11} form Mg^{2+}–Fe^{2+} solid solutions (Boffa Ballaran et al. 2015; Sinmyo et al. 2016, 2019; Ishii et al. 2018; Uenver-Thiele et al. 2018). The effect of Mg^{2+} should be studied further because the incorporation of Mg^{2+} largely decreases the electrical conductivity. Most recently, high-pressure magnesium silicate mineral $(Mg,Fe)_5Si_2O_9$ elgoresyite was found to form a solid solution of $(Mg,Fe)_5Si_2O_9$–Fe_7O_9 via the $(Mg^{2+},Fe^{2+})+Si^{4+}=2\,Fe^{3+}$ substitution (Bindi et al. 2021). While the stability of the phase is not yet clear, the electrical properties of $(Mg,Fe)_5Si_2O_9$ may be comparable to those of Fe_7O_9 because they have a similar crystal structure.

Supplementary Information The online version contains supplementary material available at https://doi.org/10.1007/s00269-022-01188-4.

Acknowledgements This work was supported by JSPS KAKENHI (Grant Number JP19H01989).

References

Akahama Y, Kawamura H (2004) High-pressure Raman spectroscopy of diamond anvils to 250 GPa: method for pressure determination in the multimegabar pressure range. J Appl Phys 96:3748–3751

Anzolini C, Marquardt K, Stagno V, Bindi L, Frost DJ, Pearson DG, Harris JW, Hemley RJ, Nestola F (2020) Evidence for complex iron oxides in the deep mantle from FeNi (Cu) inclusions in super-deep diamond. Proc Natl Acad Sci 117:21088–21094

Bindi L, Sinmyo R, Bykova E, Ovsyannikov SV, McCammon C, Kupenko I, Ismailova L, Dubrovinsky L, Xie X (2021) Discovery of elgoresyite,(Mg, Fe)$_5$Si$_2$O$_9$: implications for novel iron-magnesium silicates in rocky planetary interiors. ACS Earth Space Chem 5:2124–2130

Blakely RJ, Brocher TM, Wells RE (2005) Subduction-zone magnetic anomalies and implications for hydrated forearc mantle. Geology 33:445–448

Boffa Ballaran T, Uenver-Thiele L, Woodland AB (2015) Complete substitution of Fe^{2+} by Mg in Fe_4O_5: The crystal structure of the $Mg_2Fe_2O_5$ end-member. Am Miner 100:628–632

Bykova E, Dubrovinsky L, Dubrovinskaia N, Bykov M, McCammon C, Ovsyannikov SV, Liermann H-P, Kupenko I, Chumakov AI, Rüffer R (2016) Structural complexity of simple Fe_2O_3 at high pressures and temperatures. Nat Commun 7:1–6

Chainani A, Yokoya T, Morimoto T, Takahashi T, Todo S (1995) High-resolution photoemission spectroscopy of the Verwey transition in Fe_3O_4. Phys Rev B 51:17976

Dobson DP, Brodholt JP (2005) Subducted banded iron formations as a source of ultralow-velocity zones at the core–mantle boundary. Nature 434:371–374

Dobson DP, Richmond NC, Brodholt JP (1997) A high-temperature electrical conduction mechanism in the lower mantle phase (Mg, Fe)$_{1-x}$O. Science 275:1779–1781

Fei Y, Frost DJ, Mao H-K, Prewitt CT, Haeusermann D (1999) In situ structure determination of the high-pressure phase of Fe_3O_4. Am Miner 84:203–206

Frost DJ, Liebske C, Langenhorst F, McCammon CA, Trønnes RG, Rubie DC (2004) Experimental evidence for the existence of iron-rich metal in the Earth's lower mantle. Nature 428:409–412

Hamada M, Kamada S, Ohtani E, Mitsui T, Masuda R, Sakamaki T, Suzuki N, Maeda F, Akasaka M (2016) Magnetic and spin transitions in wüstite: a synchrotron Mössbauer spectroscopic study. Phys Rev B 93:155165

Hikosaka K, Sinmyo R, Hirose K, Ishii T, Ohishi Y (2019) The stability of Fe_5O_6 and Fe_4O_5 at high pressure and temperature. Am Mineral J Earth Planet Mater 104:1356–1359

Irifune T, Shinmei T, McCammon CA, Miyajima N, Rubie DC, Frost DJ (2010) Iron partitioning and density changes of pyrolite in Earth's lower mantle. Science 327:193–195

Ishii T, Shi L, Huang R, Tsujino N, Druzhbin D, Myhill R, Li Y, Wang L, Yamamoto T, Miyajima N (2016) Generation of pressures over 40 GPa using Kawai-type multi-anvil press with tungsten carbide anvils. Rev Scic Instrum 87:024501

Ishii T, Uenver-Thiele L, Woodland AB, Alig E, Boffa Ballaran T (2018) Synthesis and crystal structure of Mg-bearing Fe_9O_{11}: new insight in the complexity of Fe-Mg oxides at conditions of the deep upper mantle. Am Mineral J Earth Planet Mater 103:1873–1876

Ishii T, Liu Z, Katsura T (2019) A breakthrough in pressure generation by a Kawai-type multi-anvil apparatus with tungsten carbide anvils. Engineering 5(3):434–440

Kagi H, Zedgenizov DA, Ohfuji H, Ishibashi H (2016) Micro-and nano-inclusions in a superdeep diamond from São Luiz, Brazil. Geochem Int 54:834–838

Kaminsky FV, Ryabchikov ID, McCammon CA, Longo M, Abakumov AM, Turner S, Heidari H (2015) Oxidation potential in the Earth's lower mantle as recorded by ferropericlase inclusions in diamond. Earth Planet Sci Lett 417:49–56

Kang N, Schmidt MW (2017) The melting of subducted banded iron formations. Earth Planet Sci Lett 476:165–178

Katsura T, Yoneda A, Yamazaki D, Yoshino T, Ito E (2010) Adiabatic temperature profile in the mantle. Phys Earth Planet Inter 183:212–218

Katsura T, Baba K, Yoshino T, Kogiso T (2017) Electrical conductivity of the oceanic asthenosphere and its interpretation based on laboratory measurements. Tectonophysics 717:162–181

Katsura T., Yoshino T. (2015) Heterogeneity of Electrical Conductivity in the Oceanic Upper Mantle. In: Khan A, Deschamps F (eds) The Earth's Heterogeneous Mantle. Springer Geophysics. Springer, Cham. 173–204

Kiseeva ES, Vasiukov DM, Wood BJ, McCammon C, Stachel T, Bykov M, Bykova E, Chumakov A, Cerantola V, Harris JW (2018) Oxidized iron in garnets from the mantle transition zone. Nat Geosci 11:144–147

Kupenko I, Aprilis G, Vasiukov D, McCammon C, Chariton S, Cerantola V, Kantor I, Chumakov A, Rüffer R, Dubrovinsky L (2019) Magnetism in cold subducting slabs at mantle transition zone depths. Nature 570:102–106

Lavina B, Meng Y (2015) Unraveling the complexity of iron oxides at high pressure and temperature: synthesis of Fe_5O_6. Sci Adv 1:e1400260

Lavina B, Dera P, Kim E, Meng Y, Downs RT, Weck PF, Sutton SR, Zhao Y (2011) Discovery of the recoverable high-pressure iron oxide Fe_4O_5. Proc Natl Acad Sci 108:17281–17285

McCammon CA (2005) Mantle oxidation state and oxygen fugacity: constraints on mantle chemistry, structure, and dynamics. In: van der Hilst R et al. (eds) Earth's deep mantle: structure, composition and evolution., Geophysical Monographs, vol. 160. SerAGU, Washington DC, pp 219–240

Meng Y, Fei Y, Weidner D, Gwanmesia G, Hu J (1994) Hydrostatic compression of γ-Mg_2SiO_4 to mantle pressures and 700 K: thermal equation of state and related thermoelastic properties. Phys Chem Miner 21:407–412

Merlini M, Hanfland M, Salamat A, Petitgirard S, Müller H (2015) The crystal structures of $Mg_2Fe_2C_4O_{13}$, with tetrahedrally coordinated carbon, and $Fe_{13}O_{19}$, synthesized at deep mantle conditions. Am Miner 100:2001–2004

Morris ER, Williams Q (1997) Electrical resistivity of Fe_3O_4 to 48 GPa: Compression-induced changes in electron hopping at mantle pressures. J Geophys Res Solid Earth 102:18139–18148

Myhill R, Ojwang DO, Ziberna L, Frost DJ, Ballaran TB, Miyajima N (2016) On the P-T–fO_2 stability of Fe_4O_5, Fe_5O_6 and Fe_4O_5-rich solid solutions. Contrib Miner Petrol 171:1–11

Ohta K, Hirose K, Onoda S, Shimizu K (2007) The effect of iron spin transition on electrical conductivity of (Mg, Fe) O magnesiowüstite. Proc Jpn Acad Ser B 83:97–100

Ohta K, Hirose K, Shimizu K, Ohishi Y (2010) High-pressure experimental evidence for metal FeO with normal NiAs-type structure. Phys Rev B 82:174120

Ohta K, Cohen RE, Hirose K, Haule K, Shimizu K, Ohishi Y (2012) Experimental and theoretical evidence for pressure-induced metallization in FeO with rocksalt-type structure. Phys Rev Lett 108:026403

Ovsyannikov SV, Bykov M, Bykova E, Kozlenko DP, Tsirlin AA, Karkin AE, Shchennikov VV, Kichanov SE, Gou H, Abakumov AM (2016) Charge-ordering transition in iron oxide Fe_4O_5 involving competing dimer and trimer formation. Nat Chem 8:501–508

Ovsyannikov SV, Bykov M, Medvedev SA, Naumov PG, Jesche A, Tsirlin AA, Bykova E, Chuvashova I, Karkin AE, Dyadkin V (2020) A room-temperature Verwey-type transition in iron oxide, Fe_5O_6. Angew Chem 132:5681–5685

Pasternak M, Rozenberg GK, Machavariani GY, Naaman O, Taylor R, Jeanloz R (1999) Breakdown of the Mott-Hubbard state in Fe_2O_3: a first-order insulator-metal transition with collapse of magnetism at 50 GPa. Phys Rev Lett 82:4663

Pasternak MP, Taylor R, Jeanloz R, Li X, Nguyen JH, McCammon CA (1997) High pressure collapse of magnetism in $Fe_{0.94}O$: mössbauer spectroscopy beyond 100 GPa. Phys Rev Lett 79:5046

Potapkin V, McCammon C, Glazyrin K, Kantor A, Kupenko I, Prescher C, Sinmyo R, Smirnov G, Chumakov AI, Rüffer R (2013) Effect of iron oxidation state on the electrical conductivity of the Earth's lower mantle. Nat Commun 4:1–6

Püthe C, Kuvshinov A (2013) Determination of the 3-D distribution of electrical conductivity in Earth's mantle from Swarm satellite data: frequency domain approach based on inversion of induced coefficients. Earth Planets Space 65:1247–1256

Rohrbach A, Ballhaus C, Golla-Schindler U, Ulmer P, Kamenetsky VS, Kuzmin DV (2007) Metal saturation in the upper mantle. Nature 449:456–458

Senn MS, Wright JP, Attfield JP (2012) Charge order and three-site distortions in the Verwey structure of magnetite. Nature 481:173–176

Sinmyo R, Pesce G, Greenberg E, McCammon C, Dubrovinsky L (2014) Lower mantle electrical conductivity based on measurements of Al, Fe-bearing perovskite under lower mantle conditions. Earth Planet Sci Lett 393:165–172

Sinmyo R, Bykova E, Ovsyannikov SV, McCammon C, Kupenko I, Ismailova L, Dubrovinsky L (2016) Discovery of Fe_7O_9: a new iron oxide with a complex monoclinic structure. Sci Rep 6:1–7

Sinmyo R, Nakajima Y, McCammon CA, Miyajima N, Petitgirard S, Myhill R, Dubrovinsky L, Frost DJ (2019) Effect of Fe^{3+} on phase relations in the lower mantle: implications for redox melting in stagnant slabs. J Geophys Res Solid Earth 124:12484–12497

Smith EM, Shirey SB, Nestola F, Bullock ES, Wang J, Richardson SH, Wang W (2016) Large gem diamonds from metallic liquid in Earth's deep mantle. Science 354:1403–1405

Stagno V, Ojwang DO, McCammon CA, Frost DJ (2013) The oxidation state of the mantle and the extraction of carbon from Earth's interior. Nature 493:84–88

Tannhauser DS (1962) Conductivity in iron oxides. J Phys Chem Solids 23:25–34

Tsuchiya T, Wentzcovitch RM, Da Silva CR, De Gironcoli S (2006) Spin transition in magnesiowüstite in Earth's lower mantle. Phys Rev Letters 96:198501

Uenver-Thiele L, Woodland AB, Miyajima N, Ballaran TB, Frost DJ (2018) Behaviour of Fe_4O_5–$Mg_2Fe_2O_5$ solid solutions and their relation to coexisting Mg–Fe silicates and oxide phases. Contrib Miner Petrol 173:1–16

Wang Y, Weidner DJ, Zhang J, Gwanrnesia GD, Liebermann RC (1998) Thermal equation of state of garnets along the pyrope-majorite join. Phys Earth Planet Inter 105:59–71

Wirth R, Dobrzhinetskaya L, Harte B, Schreiber A, Green H (2014) High-Fe (Mg, Fe)O inclusion in diamond apparently from the lowermost mantle. Earth Planet Sci Lett 404:365–375

Woodland A, Schollenbruch K, Koch M, Ballaran TB, Angel R, Frost D (2013) Fe_4O_5 and its solid solutions in several simple systems. Contrib Miner Petrol 166:1677–1686

Xu Y, McCammon C, Poe BT (1998) The effect of alumina on the electrical conductivity of silicate perovskite. Science 282:922–924

Yang A, Qin Q, Tao X, Zhang S, Zhao Y, Zhang P (2021) Metallic nature and site-selective magnetic moment collapse in iron oxide Fe_4O_5 at the extreme conditions of Earth's deep interior. Phys Lett A 127607

Yoshino T (2010) Laboratory electrical conductivity measurement of mantle minerals. Surv Geophys 31:163–206

Yoshino T, Katsura T (2009) Effect of iron content on electrical conductivity of ringwoodite, with implications for electrical structure in the transition zone. Phys Earth Planet Inter 174:3–9

Yoshino T, Nishi M, Matsuzaki T, Yamazaki D, Katsura T (2008) Electrical conductivity of majorite garnet and its implications for electrical structure in the mantle transition zone. Phys Earth Planet Inter 170:193–200

Yoshino T, Kamada S, Zhao C, Ohtani E, Hirao N (2016) Electrical conductivity model of Al-bearing bridgmanite with implications for the electrical structure of the Earth's lower mantle. Earth Planet Sci Lett 434:208–219